Biochimica et Biophysica Acta 1859 (2017) 368–376

Contents lists available at ScienceDirect

Biochimica et Biophysica Acta

journal homepage: www.elsevier.com/locate/bbamem

Role of the H-bond between L53 and T56 for Aquaporin-4 epitope in Neuromyelitis Optica

Francesco Pisani [a], Laura Simone [a,b], Concetta Domenica Gargano [a], Manuela De Bellis [a], Antonio Cibelli [a], Maria Grazia Mola [a], Giacomo Catacchio [a], Antonio Frigeri [c,d], Maria Svelto [a,e,f], Grazia Paola Nicchia [a,d,*]

[a] Department of Bioscience, Biotechnologies and Biopharmaceutics and Centre of Excellence in Comparative Genomics, University of Bari "Aldo Moro", Bari, Italy
[b] IRCCS "Casa Sollievo della Sofferenza", Research Hospital, San Giovanni Rotondo, Foggia, Italy
[c] School of Medicine, Basic Medical Sciences, Neuroscience and Sense Organs, University of Bari "Aldo Moro", Bari, Italy
[d] Department of Neuroscience, Albert Einstein College of Medicine, Yeshiva University, Bronx, NY, USA
[e] Institute of Biomembranes and Bioenergetics, National Research Council, Bari, Italy
[f] National Institute of Biostructures and Biosystems (INBB), Rome, Italy

ARTICLE INFO

Article history:
Received 6 September 2016
Received in revised form 13 December 2016
Accepted 23 December 2016
Available online 24 December 2016

Keywords:
Aquaporin-4
NMO
Molecular dynamics
OAPs
AQP4-IgG

ABSTRACT

Aquaporin-4 (AQP4) is the CNS water channel organized into well-ordered protein aggregates called Orthogonal Arrays of Particles (OAPs). Neuromyelitis Optica (NMO) is an autoimmune disease caused by anti-OAP autoantibodies (AQP4-IgG). Molecular Dynamics (MD) simulations have identified an H-bond between L53 and T56 as the key for AQP4 epitope and therefore of potential interest for drug design in NMO field.
In the present study, we have experimentally tested this MD-prediction using the classic mutagenesis approach. We substituted T56 with V56 and tested this mutant for AQP4 aggregates and AQP4-IgG binding. gSTED super-resolution microscopy showed that the mutation does not affect AQP4 aggregate dimension; immunofluorescence and cytofluorimetric analysis demonstrated its unaltered AQP4-IgG binding, therefore invalidating the MD-prediction.
We later investigated whether AQP4, expressed in Sf9 insect and HEK-293F cells, is able to correctly aggregate before and after the purification steps usually applied to obtain AQP4 crystal. The results demonstrated that AQP4-IgG recognizes AQP4 expressed in Sf9 and HEK-293F cells by immunofluorescence even though BN-PAGE analysis showed that AQP4 forms smaller aggregates when expressed in insect cells compared to mammalian cell lines. Notably, after AQP4 purification, from both insect and HEK-293F cells, no aggregates are detectable by BN-PAGE and AQP4-IgG binding is impaired in sandwich ELISA assays.
All together these results indicate that 1) the MD prediction under analysis is not supported by experimental data and 2) the procedure to obtain AQP4 crystals might affect its native architecture and, as a consequence, MD simulations. In conclusion, given the complex nature of the AQP4 epitope, MD might not be the suitable for molecular medicine advances in NMO.

1. Introduction

Water homeostasis is fundamental in the Central Nervous System (CNS) and is sustained by water channel proteins, called Aquaporins (AQPs), concentrated at the glial endfeet [1,2] facing the blood-brain and CSF-brain barriers [3,4]. AQPs allow fast water movement through the plasma membrane therefore controlling the tissue water homeostasis.

AQP monomers are formed by six transmembrane helical domains, two intracellular (B and D) and three extracellular (A, C and E) loops [5,6]. Differently from ion channels, in which the pore is formed by the monomer assembly into tetramers [7], each AQP monomer is provided with a water pore although the tetramer represents the functional unit.

The glial water channel, Aquaporin-4 (AQP4), is characterized by a higher level of plasma membrane organization in which AQP4 tetramers further aggregate into well-ordered squared structures, visible by freeze fracture electron microscopy [8], and called Orthogonal Arrays of Particles (OAPs) [2,9,10]. Aggregation of AQP4 teteramers into OAPs [9,10] confers a considerable level of protein stability necessary for their polarized expression at glial endfoot microdomains, not provided with tight junctions [2].

* Corresponding author at: Department of Bioscience, Biotechnologies and Biopharmaceutics and Centre of Excellence in Comparative Genomics, University of Bari "Aldo Moro", Via Orabona, 4, 70126 Bari, Italy.
E-mail address: graziapaola.nicchia@uniba.it (G.P. Nicchia).

http://dx.doi.org/10.1016/j.bbamem.2016.12.018
0005-2736/

Neuromyelitis Optica (NMO) is an AQP4-related neuroinflammatory disease that in recent years has brought up the importance of AQP4 structural organization in OAPs. Anti-AQP4-OAP autoantibodies (AQP4-IgG) are in fact responsible for immune-mediated pathology [11–14] and are an important biological marker for NMO diagnosis [15,16]. Elucidating the molecular mechanisms at the root of AQP4 IgG-OAP interaction is important to provide a basis for a specific therapy based on preventing the autoantibody binding to its target. In fact, although the NMO autoantibody antigen has been identified to be the AQP4 water channel, currently used therapies are not specific for NMO. They include classical broad approaches, such as immunomodulation, immunosuppression and plasmapheresis [17].

In previous studies we have shown the existence of at least two major groups of AQP4-IgG, based on the conformational epitope recognized [14] within the OAPs. Interestingly, we have also identified a single point mutation, at the base of loop A, in which the substitution of Aspartate 69 with Histidine (D69H), impairs AQP4-IgG binding and complement dependent cytotoxicity (CDC), maintaining water transport and OAP assembly properties unaltered [18]. Another group has since confirmed the importance of D69 amino acid for AQP4-IgG epitope structure [19], supporting the idea that D69 plays a pivotal role in AQP4-IgG epitope assembly.

From preliminary Molecular Dynamics (MD) simulation analysis, we found that an increased mobility of loop A induced by D69H mutation impaired epitope formation [18]. A more detailed MD simulation was later applied by Mangiatordi et al. [20] to model the mechanism responsible for D69H dependent loop A conformational change. In this study, the authors propose that D69H induces a domino effect in which the H-bond interaction between the oxygen atom of the carbonyl of the backbone of Leucin 53 (L53) and the oxydril group of the Threonine 56 (T56) lateral chain, at the base of extracellular loop A, is substantially weakened. This event induces a conformational change of the Threonine 62 (T62) lateral chain, in the centre of loop A, responsible for loop A reorientation (Fig. 1A) and impaired AQP4-IgG binding in the D69H mutant. This very intriguing model suggests that this H-bond could be a novel target for new NMO-specific pharmacological approaches based on changing the conformational dynamics of loop A to prevent AQP4-IgG binding.

In the present study we have experimentally tested this MD simulation, here called the "H-bond hypothesis" using the classic mutagenesis approach. The data obtained does not confirm the MD model and shows that the H-bond under analysis does not play a role in AQP4-IgG binding. We also provide data suggesting the possibility that the purification steps necessary to obtain AQP4 crystals might affect its native supra-molecular architecture. Based on the experimental failure of the H-bond hypothesis and on possible problems related with OAP integrity after AQP4 purification steps, we here discuss the suitability of a molecular dynamics approach to investigate AQP4-OAP structure and AQP4 epitope molecular feature.

2. Methods

2.1. Primary amino acid sequence multiple alignment analysis

The multiple alignment analysis of human, monkey, rat and mouse AQP4 primary amino acid sequences was performed using the Clustal Omega (www.ebi.ac.uk/Tools/msa/clustalo/). All the sequences were obtained from NCBI, Entrez Gene, Reference Sequences.

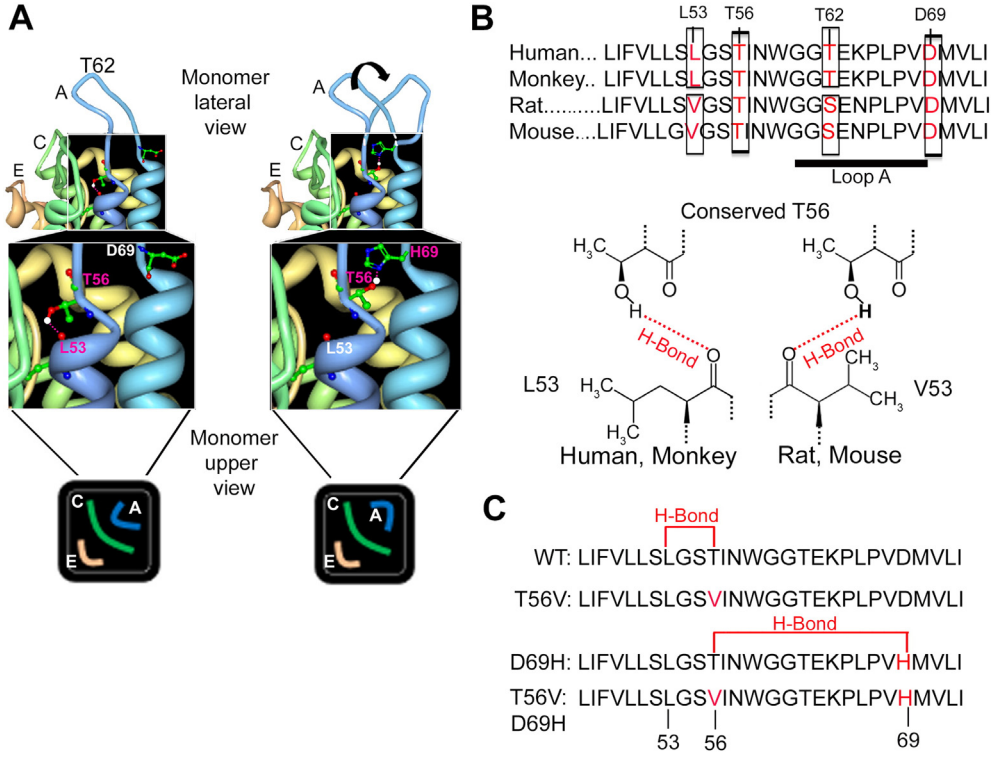

Fig. 1. Rationale of the mutagenesis approach used to verify the H-bond hypothesis. A) Predicted effect of D69H on T56 and L53 interaction by MD: H69 would reorient loop A by weakening the strength of the H-bond interaction between L53 and T56. B) Multialignment analysis of human, monkey, rat and mouse AQP4 primary sequence. Top: T56 and D69 are conserved while human and monkey L53 and T62 are substituted by V53 and S62, respectively, in rat and mouse. Bottom: The hydrogen bond formed by L53 or V53 with T56. C) Description of AQP4 mutants generated to verify the H-bond hypothesis. From top to bottom: AQP4 WT sequence, AQP4 T56V point mutation, AQP4 D69H point mutation and AQP4 T56VD69H double mutant. T56V is the mutant for WT in which the presence of Val56 impairs the H-bond under analysis, indicated in red. Similarly, T56V-D69H is the mutant for D69H in which Val56 impairs the H-bond under analysis, indicated in red.

2.2. Constructs and site-specific mutagenesis

Human AQP4-M23, and AQP4-M23 with a C-terminal 6xHis tag CDSs were cloned into pTarget (Promega, www.Promega.com) and pmCherry-N1 (Clontech, www.Clontech.com) vectors. All the AQP4-M23 mutants were obtained with a site-specific mutagenesis approach using QuikChange II site-directed mutagenesis kit (Stratagene, www.Agilent.com) according to the instruction manual. Briefly, the AQP4-M23 isoforms were cloned and used as template in a long high fidelity PCR performed with Pfu Ultra high fidelity DNA polymerase. The site-specific mutant primers were designed using the web-based QuikChange primer design program from Stratagene available on line. All constructs were fully sequenced.

2.3. Cells and transfection

HEK293 (human embryonic kidney) and U87MG cells were seeded the day before transfection. Transient transfection was carried out using Lipofectamine 2000 (Invitrogen, www.thermofisher.com) in OptiMEM growth medium. The medium was replaced after 8 h with Dulbecco Modified Eagle's Medium (DMEM), 10% fetal bovine serum (FBS), 100 U/ml penicillin, 100 mg/ml streptomycin, and maintained at 37 °C in a 5% CO_2 incubator. HEK293-F cells were cultured in suspension using FreeStyle™ 293 Expression Medium and transfected in according with manual instruction (FreeStyle™ 293-F, Invitrogen, www.thermofisher.com).

2.4. Antibodies

Anti-AQP4 antibodies and secondary antibodies were from Santa Cruz Biotechnology (www.scbt.com). The secondary antibody used for immunoblotting was a donkey anti-goat IgG peroxidase conjugated, for immunofluorescence analysis it was a donkey anti-goat or goat anti-human Alexa 488-conjugate.

2.5. Patient sera

All subjects gave their written informed consent to the study, which was approved by the institutional ethics committee of the University of Bari. Three NMO sera, representative of major epitopes categories [14] were used.

2.6. Cell based assay (CBA)

CBA test and end-point titre assay were conducted as previously described [16]. CBA for AQP4-IgG binding was performed using live HEK cells, transfected with mCherry-tagged AQP4 mutants, in PBSCa^{2+} Mg^{2+} 0.1% gelatin, using NMO serum, at RT for 1 h. After incubation with NMO serum, cells were washed and secondary antibody was added. Cells were washed, fixed for 10 min with 4% formaldehyde in PBS and finally mounted in PBS-glycerol (1:1), pH 8.0, containing 1% *n*-propyl gallate.

2.7. Immunofluorescence for Gated Stimulated Emission Depletion (gSTED) super resolution microscopy and measure of aggregate size

Immunofluorescence for gSTED was performed as reported in the Quick Guide to STED Sample Preparation (http://www.leica-microsystems.com). Briefly, cells were washed in PBS, fixed with 2% PFA for 10 min, permeabilized with 0.3% Triton X-100 for 10 min, saturated with 2% BSA and incubated with anti-AQP4 antibody in 2% BSA. After washings, cells were incubated with secondary anti-goat Alexa Fluor488-conjugate in 2% BSA, washed with PBS and finally mounted with mowiol. For image acquisition and analysis, a Leica TCS SP8 STED 3× microscope and Leica LASX software were used (http://www.leica-microsystems.com). A Leica HC PL APO 100×/1.40 Oil STED White objective and Type F Immersion liquid with 1.5 refractive index were used. Excitation of Alexa-Fluor488 dye was performed with a continuous wave 488 nm wavelength diode laser with a maximum light output in the focal plane of 10 mW (NKT Photonics sign supercontinuum laser (http://www.nktphotonics.com). The depletion was performed using a continuous wave 592 nm wavelength fiber laser with a maximum light output in the focal plane of <0.5 mW (http://www.laserquantum.com). gSTED images were deconvoluted using Huygens Professional Software (https://svi.nl/HuygensProfessional) and the deconvoluted images were used to determine AQP4 aggregate size. For determination of the AQP4 aggregate size, random areas were selected from representative images and an intensity profile was plotted for each aggregate using the "determine FWHM" function in Leica LASX software. The width of the profile at half-maximal intensity was measured as cluster size (Full Width at Half Maximum (FWHM)) as reported [21]. At least one hundred clusters per area were measured.

2.8. Sample preparation and cytofluorimetry

Transient transfected cells were washed three times with PBS and harvested with trypsin (Euroclone, www.euroclonegroup.it). 1×10^6 cells were incubated with NMO patient sera for 45 min in rotation at room temperature. Cells were subsequently washed, and bound human IgG were detected with Alexa-Fluor488 conjugated goat anti-human antibody for 30 min, in rotation at room temperature in the dark. Cells were washed again, re-suspended in filtered PBS added with 1 mM EDTA, 25 mM HEPES, 1% Fetal Bovine Serum. To obtain a single cell suspension, large debris and cell clusters were removed from the cell suspension by filtration through pre-wetted syringe type 50 μm filcon filters (Falcon, BD Biosciences, www.bdbiosciences.com) into 5 ml tubes, and analyzed by flow cytometry. A FACS Aria III (BD Biosciences, www.bdbiosciences.com) instrument was used for flow cytometry analysis. Negative controls were represented by non-transfected cells. A small portion of transfected and non-transfected cells was mixed with goat anti-human Alexa-Fluor488-conjugate secondary antibody missing the previous incubation with NMO patient sera to set the maximum threshold for non-specific binding. Cells were first gated according to their light scattering characteristics (forward scatter: FCS; side scatter: SSC), and according to mCherry expression (PE-A channel). The population positive to mCherry, was then analyzed to detect human AQP4-IgG binding through fluorescence emission detected on the FITC channel. Flow cytometry analysis was conducted with FACS Diva 8.0 software (BD Biosciences, www.bdbiosciences.com).

2.9. Recombinant AQP4 expression and native purification

Human AQP4-M23 isoform with C-terminal 6XHis tag was expressed using the Bac-to-Bac expression system (www.thermofisher.com) in *Spodoptera frugiperda* cells, or in HEK293-F suspension culture (www.thermofisher.com) according to the instruction manual. Cell membranes were obtained as reported and solubilized in native buffer containing 2% *n*-Dodecyl β-D-maltoside (DDM), 10% glycerol, 5 mM imidazole pH 7.4, 300 mM NaCl and protease inhibitor cocktail as reported [22]. His-tagged AQP4 was purified by Nickel based chromatography using Ni^{2+} NTA-Agarose (QIAGEN, www.qiagen.com), washed and eluted with the same buffer used for extraction with 20 mM and 250 mM imidazole, respectively. Native purified AQP4 was immediately dialyzed in 2% *n*-Dodecyl β-D-maltoside (DDM), 10% glycerol, 5 mM imidazole pH 7.4, 300 mM NaCl, to eliminate excess of imidazole and checked by SDS-PAGE and Coomassie staining, quantified by Micro-BCA Protein Assay Kit (Thermo, www.thermofisher.com) and used for Blue-Native PAGE analysis and sandwich ELISA.

2.10. Blue Native PAGE

Blue Native PAGE was performed using pre-cast NativePAGE™ Novex™ 3–12% Bis-Tris Protein Gels, Thermo Fisher (www.thermofisher.com) according to the instruction manual. Transfected U87, infected Sf9 or HEK-293F membrane vesicles cells were extracted in BN-buffer (1% Triton X-100, 12 mM NaCl, 500 mM 6-aminohexanoic acid, 20 mM BisTris, pH 7.0, 2 mM EDTA, 10% glycerol) as reported [2], while purified AQP4 was diluted in BN-buffer and loaded into the gel.

2.11. AQP4-IgG sandwich ELISA with NMO sera

The NMO ELISA was performed as previously described [22]. Absorbance was read using a FlexStation3 (Molecular Devices, www.moleculardevices.com). AQP4-IgG/AQP4 absorbance was calculated as NMO normalized absorbance/AQP4 normalized absorbance. AQP4 normalized absorbance was calculated as reported in the next paragraph. Where reported, the wells were incubated with membrane vesicle extracts (20 μg/well).

2.12. AQP4 sandwich ELISA with commercial antibodies

To detect the amount of AQP4 coating the wells, AQP4-OAP-ELISA was performed using 0.2 μg/well of commercial rabbit anti-AQP4 in the first coating step. Goat anti-AQP4 antibody and the anti-Goat Biotin (Millipore, www.merckmillipore.com) were used.

2.13. Immunofluorescence with NMO sera using Sf9 and HEK293-Fcells

AQP4-M23 with C-terminal 6xHis expressing Sf9 cells were washed three times in Sf900II medium (Thermo Fisher, https://www.thermofisher.com) incubated in rotation with high titre NMO serum 1:1000 for 1 h, washed three times in Sf900II medium, incubated with 1:1000 Alexa-Fluor488 conjugated goat anti-human antibody for 30 min in rotation at room temperature in the dark, washed and analyzed by epifluorescence microscopy. The same procedure was used for HEK293-F cells, using the "Free style expression medium" (www.thermofisher.com) to perform incubations and washes.

2.14. Data analysis

Statistical significance was evaluated using the 2-way ANOVA and Bonferroni post-hoc test. Prism 5 GraphPad Software (San Diego, www.graphpad.com) was used. Differences with $P < 0.05$ were considered significant. The data is reported as mean with 95% confidence interval.

3. Results

3.1. Generation of mutants to validate the importance of the L53-T56 H bond for AQP4-IgG binding

Fig. 1A summarizes the H-bond MD hypothesis [20], here under analysis, proposing that a) the T56 oxydril group and the oxygen atom of the carbonyl of L53 backbone form an H-bond which is the key for the correct orientation of loop A, and b) that D69H point mutation induces the loss of this interaction, the generation of a new H-bond between H69 and T56, with consequent loop A reorientation and impaired antigen-autoantibody binding. We have here tested this MD based "H-bond hypothesis" using the classic mutagenesis approach. First, we performed a multiple alignment analysis of AQP4 sequence from human, monkey, rat and mouse (Fig. 1B top), all sequences known to be recognized by AQP4-IgG although in some cases with a different affinity between mouse and human [11,22,23]. The analysis showed that T56 and D69 are conserved, while L53 and T62 are not. L53 is specific for the human and monkey sequences but it is substituted by V53 in rat and mouse. The presence of V53, instead of L53, would still be compatible with the hypothesis since the H-bond involves the oxygen atom of the carbonyl of the backbone (Fig. 1B bottom). T62 is also specific for human and monkey but it is substituted by S62, in rat and mouse. Also in this case, the substitution of T62 with the similar amino acid S62, is still compatible with the hypothesis to be tested. The mutagenesis approach was performed, as described in Fig. 1C, using human AQP4 sequence. Two mutants were generated, both aimed at breaking the two H-bonds proposed to play a key role in the correct orientation of loop A and its reorientation, respectively. In particular, T56V was generated as the mutant form of WT-AQP4, in which the substitution of T56 with V56 is incompatible with the formation of the H-bond with L53. T56V-D69H double mutant was generated as the mutant form of the already characterized D69H [18]. Similarly, the presence of V56 in this mutant does not allow the formation of an H-bond between V56 and H69.

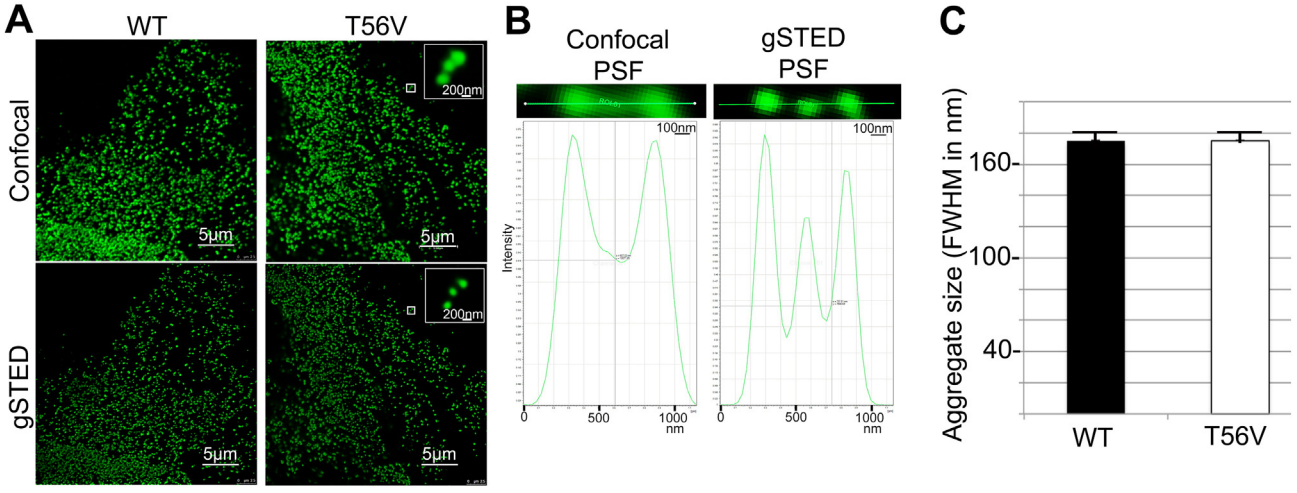

Fig. 2. AQP4 plasma membrane aggregate size measured by gSTED microscopy A) Representative images of WT and T56V transfected cells, stained with anti-AQP4 commercial antibodies, obtained by confocal and gSTED microscopy. Inset: higher magnification of the same area visualized by confocal and gSTED microscopy. Scale bar: 5 μm (inset: 200 nm). B) Representative images (top) and relative intensity fluorescence profiles (bottom) of AQP4 aggregates (WT) by confocal (left) and gSTED (right) microscopy, highlighting the improved resolution by gSTED. One large area of 1 μm with two main peaks observed in confocal microscopy is resolved in three different AQP4 aggregates by gSTED. Scale bar: 100 nm. C) Histogram showing no difference between AQP4 plasma membrane aggregate size of WT and T56V AQP4 expressed in Full Width at Half Maximum (FWHM).

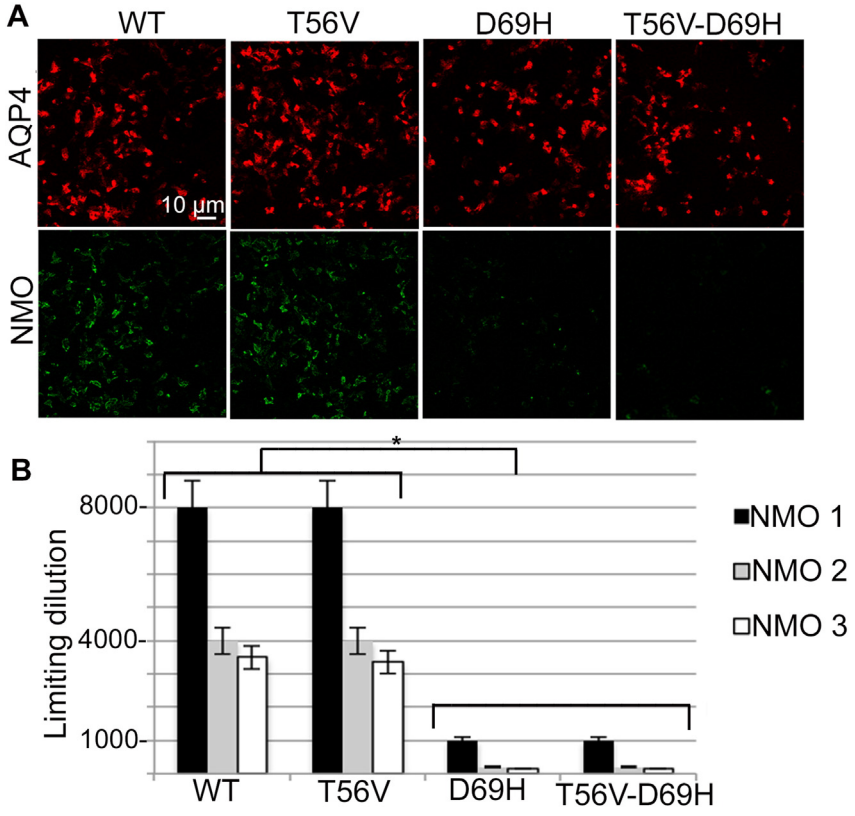

Fig. 3. AQP4-IgG binding to WT and mutant AQP4 expressing cells by end point titre cell based assay. A) Representative immunofluorescence performed with AQP4-IgG containing serum (NMO, in green) on cells transfected with cherry tagged WT and mutated AQP4 (in red). Scale bar: 10 μm. B) Histogram showing the end-point titre (limiting dilution) of three different AQP4-IgG containing NMO sera (NMO1, NMO2, NMO3) measured by cell based assay on WT and mutated AQP4, as indicated (*P < 0.001, n = 4).

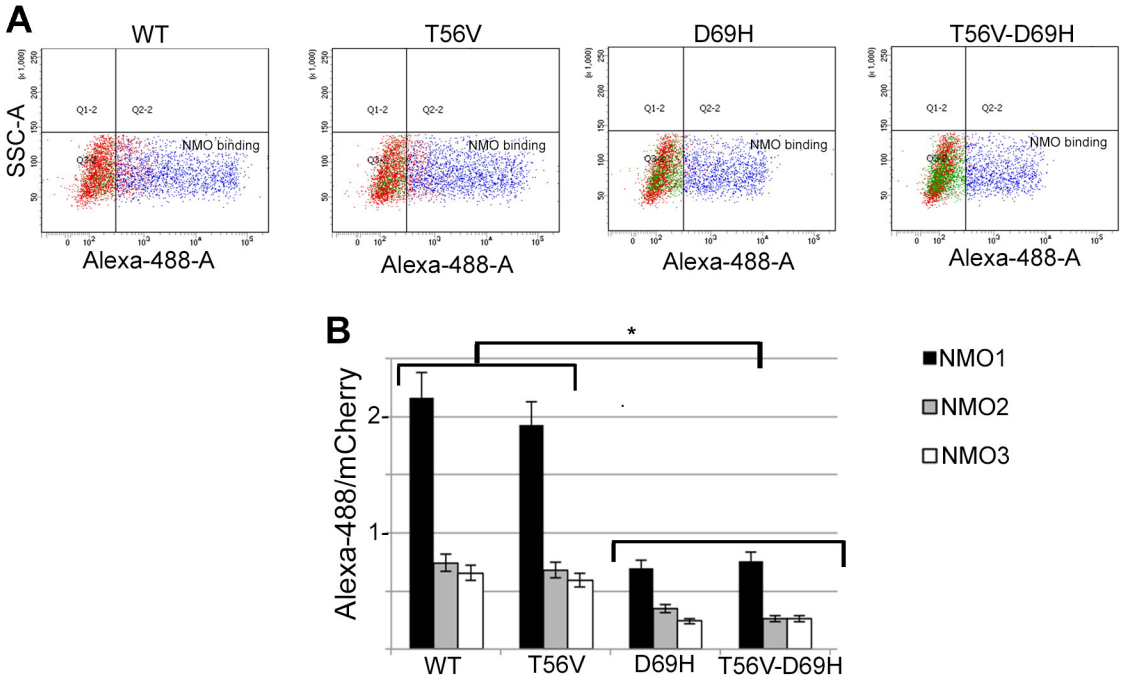

Fig. 4. AQP4-IgG binding to WT and mutated AQP4 expressing cells by cytofluorimetric analysis. A) Representative cytofluorimetric dot plot analysis of AQP4-IgG binding (Alexa-488-A) and SSC-A using cherry tagged - AQP4 (WT or mutated) expressing HEK cells. The negative events are shown in red, the events positive for AQP4 and negative for NMO serum are shown in green; the events positive for both AQP4 and NMO serum are shown in blue. B) Histogram showing the quantitative analysis of AQP4-IgG binding affinity for WT and mutated AQP4 evaluated using three different AQP4-IgG containing sera, diluted as follows: NMO1 1:4000, NMO2 1:1000, NMO3 1:1000, by Alexa-488/mCherry signal (*P < 0.001, n = 4).

3.2. A T56-L53 H-bond is not essential for AQP4 to aggregate into supramolecular structures

AQP4-IgG recognizes AQP4 organized into OAPs [11,16] therefore, we first evaluated whether impairing the T56-L53 H-bond affects AQP4 supramolecular assembly in the plasma membrane (Fig. 2). In particular, potential differences in AQP4 aggregate size between WT and T56V mutants were investigated by the use of gated STED (gSTED) microscopy, a super resolution technique giving a resolution close to 30 nm [21]. For this analysis HEK cells were transfected with

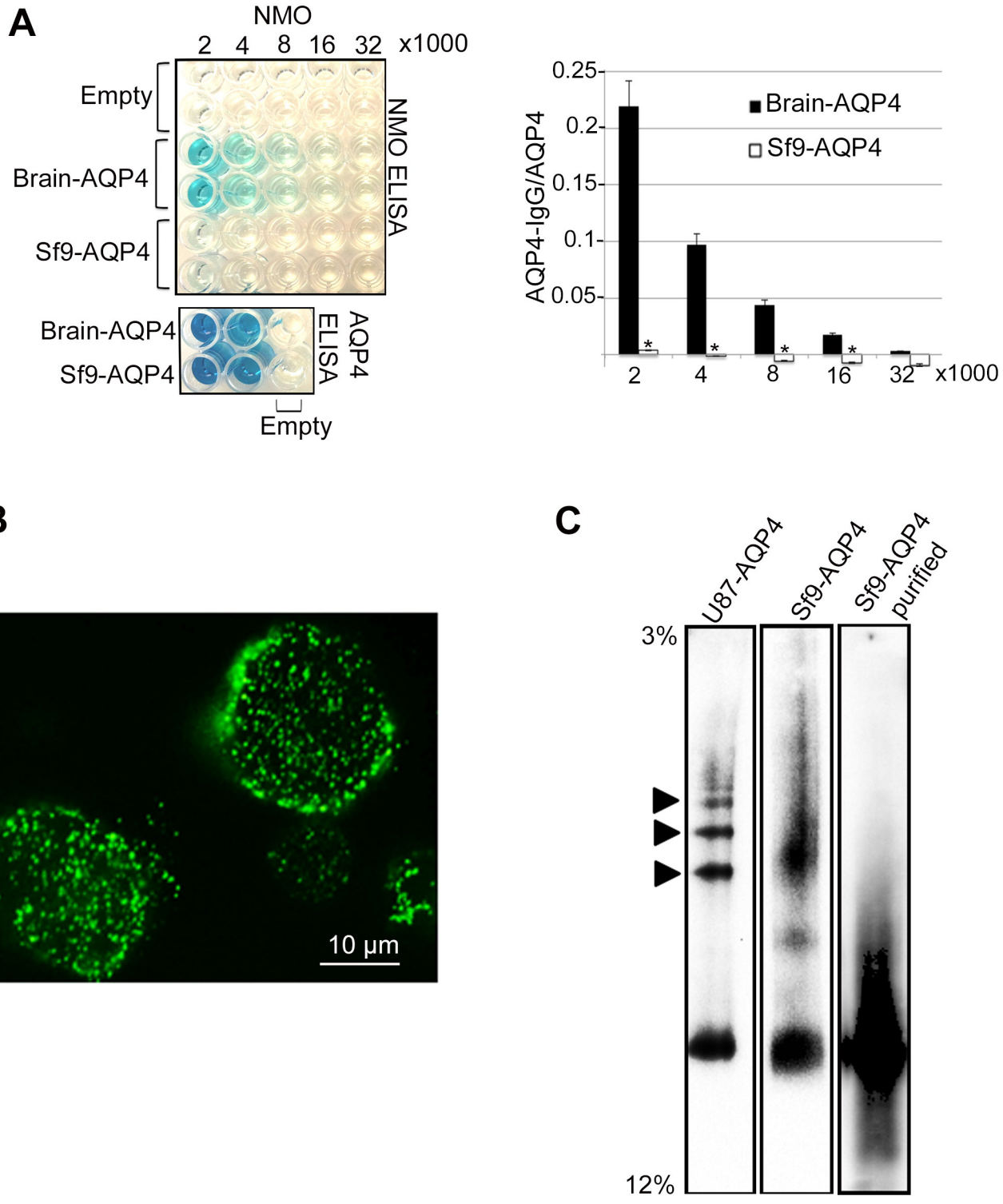

Fig. 5. AQP4 supramolecular structures in Sf9 insect cells. A) Left, plate of a sandwich ELISA performed with native AQP4 purified from rat brain (Brain-AQP4) and recombinant AQP4 purified from Sf9 insect cells (Sf9-AQP4), using high titre NMO-1 serum (NMO ELISA) and commercial anti-AQP4 (AQP4 ELISA). The dilution ranging from 1:2000 to 1:32,000 is indicated (2 to 32). Right, absorbance analysis of sandwich ELISA. Note that AQP4 purified from AQP4 expressing Sf9 insect cells is not recognized by AQP4-IgG (*$P < 0.001$, $n = 4$). B) Immunofluorescence performed with AQP4 IgG containing NMO serum on His-tagged AQP4 expressing Sf9 insect cells (AQP4-Sf9). AQP4-IgG recognizes the recombinant human protein at the plasma membrane level (green dotted staining). C) Immunoblotting performed with AQP4 commercial antibody after BN-PAGE on the following samples: lysate of U87 cells expressing His tagged-AQP4 (U87-AQP4), membrane vesicles of Sf9 expressing His tagged-AQP4 (Sf9-AQP4) and AQP4 purified from Sf9 cells (Sf9-AQP4 purified). The arrowheads indicate the presence of AQP4 high molecular weight aggregates in U87 cells. The aggregates are altered in Sf9 cells and very small after AQP4 purification.

WT and T56V AQP4 M23 isoform, corresponding to the OAP forming isoform. The comparison of the gSTED with the confocal analysis is shown in Fig. 2A to demonstrate the higher resolution obtained with gSTED therefore suitable for the analysis of isolated AQP4 aggregates resembling OAPs (Fig. 2B). AQP4 aggregate dimension was measured for WT and T56V on isolated fluorescent spots (Fig. 2C). The data demonstrate that the mutation T56V does not affect AQP4 aggregate dimension, suggesting that the MD-predicted H-bond has no crucial role into AQP4 supramolecular assembly.

3.3. The T56 and L53 H-bond is not essential for AQP4-IgG binding

The normal T56V AQP4 aggregation into supramolecular structures is not necessarily related with its preserved capability to bind AQP4-IgG, as already reported [18]. The MD-predicted interaction between T56 and L53 as a key for the OAP epitope was then verified using AQP4 mutants described in Fig. 1. HEK cells were transiently transfected with mCherry tagged WT or mutated AQP4 and AQP4-IgG binding was evaluated using end-point titre cell-based assay (CBA) [16] and cytofluorimetric analysis (Fig. 3 and Fig. 4). Three AQP4-IgG positive NMO patient sera, representative of major conformational epitope categories [14] were used. End-point titre CBA showed that all NMO sera tested were able to bind WT and T56V with same affinity (Fig. 3), therefore disproving the H-bond hypothesis. AQP4-IgG affinity for D69H was reduced, as already reported [18], and comparable between D69H and T56V-D69H. This indicated that, in the presence of D69H mutation, the H-bond between T56 and H69 does not play any role in the context analyzed, as expected by MD simulations [20].

The semi-quantitative analysis obtained by fluorescence microscopy based end-point titre CBA [16] was further implemented by a quantitative analysis performed using cytofluorimetry on live HEK cells transfected with mCherry tagged WT or mutated AQP4 (Fig. 4). AQP4-IgG affinity for AQP4 (WT and mutants) was measured by the cytofluorimetric Alexa488/mCherry median ratio to normalize AQP4-IgG binding with the level of expression of AQP4 sequences under analysis. The results were consistent for the three NMO sera analyzed in showing that AQP4-IgG binding was preserved in the T56V compared to WT AQP4, and that no modification of AQP4-IgG binding was observed for the double mutant T56V-D69H compared with D69H. These data, although limited to only three sera, demonstrate that the MD predicted H-bond is not crucial for AQP4 epitope assembly.

3.4. AQP4 epitope is impaired during AQP4 purification procedures

MD simulation studies here under analysis have been based on AQP4 crystal coordinates [20] obtained from purified AQP4 [24]. We therefore wanted to analyze if the failure of MD prediction could be somehow related to crystal coordinates. First, we tested whether the AQP4 epitope is maintained during AQP4 purification procedures. To this end we performed a sandwich ELISA in which AQP4-IgG binding to native AQP4 enriched from rat brain by nSEC [22] and recombinant AQP4 purified from Sf9 insect cells were compared (Fig. 5A). The results show that recombinant AQP4 purified from insect cells was ineffective when compared to native AQP4 enriched from rat brain in the ELISA assay. The analysis was therefore focused on expression of recombinant AQP4 in Sf9 cells. Fig. 5 B shows that AQP4 IgG recognizes AQP4 by immunofluorescence, indicating that AQP4 is able to aggregate into OAPs in Sf9 cells. However, the analysis of AQP4 supramolecular structures, revealed by BN/PAGE-immunoblotting (Fig. 5C) demonstrated the altered pattern of the AQP4 aggregation state in Sf9 cells. In particular, aggregates of recombinant (His-tagged) AQP4 expressed in insect cells were smaller compared to those of recombinant (His-tagged) AQP4 expressed in mammalian cells (U87). Moreover, the higher molecular weight AQP4 aggregates became even smaller after the purification steps. These results explain why AQP4 IgG does not recognize AQP4 purified from insect cells in sandwich ELISA. To ascertain whether the non-mammalian source of AQP4 protein could be involved in the failure of AQP4 IgG binding shown in Fig. 5, we expressed AQP4 in the human cell line HEK-293F, able to grow in suspension (Fig. 6), therefore more suitable for protein purification procedures. The results obtained showed that AQP4 is recognized by AQP4-IgG by immunofluorescence analysis (Fig. 6A), as expected. However, BN-PAGE revealed that AQP4 is not able to assemble in supramolecular structures after the purification procedures, while these are visible in AQP4 transfected HEK-293F protein extract (Fig. 6B). The same samples, analyzed in BN-PAGE, were finally tested for AQP4-IgG binding in sandwich ELISA. The results in Fig. 6C show that AQP4 IgG does not recognize AQP4 after the purification procedures, in line with BN-PAGE data.

4. Discussion

There are a number of examples of MD simulations later validated by experimental data [25], however, it is generally accepted that in silico

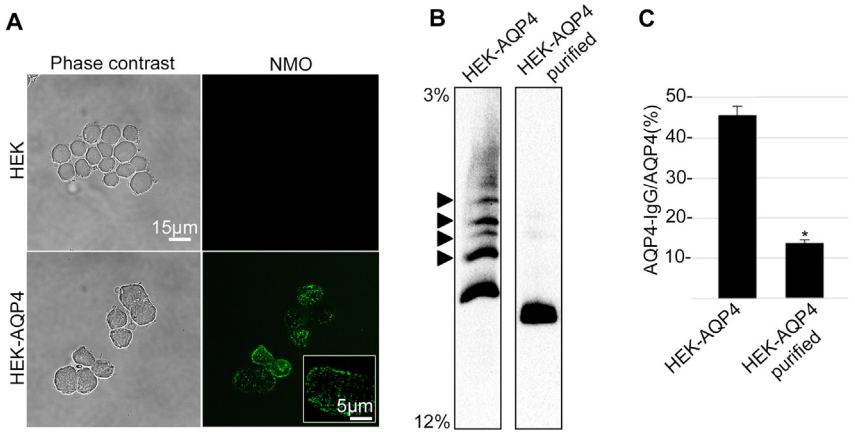

Fig. 6. AQP4 supramolecular structure in HEK-293F human cells. A) Phase contrast images (Phase contrast) and immunofluorescence analysis performed with AQP4 IgG containing NMO serum (NMO) on His-tagged AQP4 expressing HEK-293F human cells (HEK-AQP4) and untransfected cells (HEK). AQP4-IgG recognizes the recombinant human protein at the plasma membrane level (green dotted staining). B) Immunoblotting performed with AQP4 commercial antibody after BN-PAGE on His-tagged AQP4 expressing HEK-293F cell protein extract (HEK-AQP4) and AQP4 protein after the purification procedures (HEK-AQP4 purified). The arrowheads indicate AQP4 supramolecular structures visible in the protein extracts and absent after the purification procedures. C) Histogram showing the absorbance analysis of sandwich ELISA in which His-tagged AQP4 expressing HEK-293F cell protein extract (HEK-AQP4) and AQP4 protein after the purification procedures (HEK-AQP4 purified) were compared for AQP4-IgG binding using high titre NMO-1 serum (AQP4-IgG) and commercial anti-AQP4 (AQP4). Data is shown as AQP4 IgG/AQP4 ratio (*$P < 0.001$, $n = 4$).

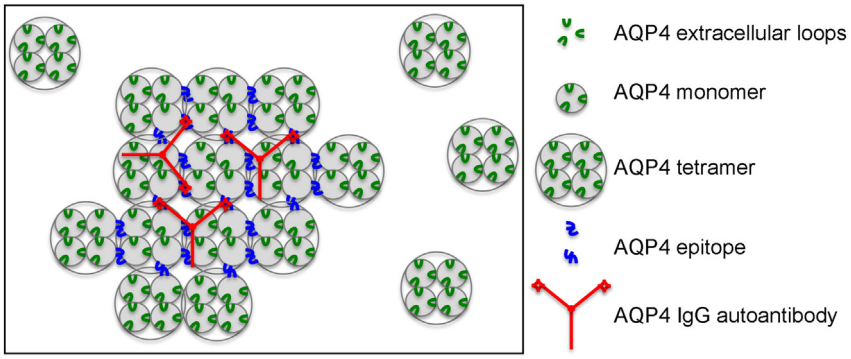

Fig. 7. Mechanism describing AQP4 epitope formation. The scheme, based on previous studies [14], shows how AQP4 tetramer aggregation induces the formation of interaction between the extracellular loops, their reorientation and AQP4 epitope formation.

models are not considered valid until verified by classic wet experiments. The present study attempted to experimentally verify the MD based H-bond hypothesis [20] stating that the H-bond between L53 and T56 is a key element for AQP4 epitope formation and therefore potential target for focused design of modulators specifically affecting AQP4 IgG binding without altering brain water homeostasis. By site-directed mutagenesis, followed by AQP4-IgG binding experiments and super-resolution fluorescence microscopy analysis, we here provide evidence against this hypothesis, by showing that the oxydril group of the T56 lateral chain has no pivotal role in AQP4-epitope assembly.

MD simulations are currently used to explore molecules of medical interest for the obvious expectations in drug discovery. The present study, however, raises some broad considerations applicable to similar situations in which a high level of molecular complexity is in conflict with the significant level of simplification needed during MD simulation. A general simple issue is the molecular environment in which the protein behavior is calculated, such as the lipid composition of the cell membrane. In the case of AQP4, only the presence of 1-palmitoyl,2-oleoyl-sn-glycero-3-phosphocholine has been simulated [20], underestimating the contribution of other lipids and of other membrane proteins. However, a more specific, and in our opinion, the key issue, that could explain the failure of MD prediction, is that all MD data are computed on an AQP4 monomer. Such calculation does not take into account that the AQP4 epitope is formed by the complex interactions occurring between the extracellular loops of AQP4 tetramers, as already demonstrated [14]. Therefore, if the final AQP4 crystal structure is, for instance, valuable to study the biophysics property of the water pore, it is not suitable for modeling a three-dimensional epitope [13,26] which is the consequence of AQP4 tetramer aggregation as shown in Fig. 7. We conclude that an MD simulation on AQP4 monomer, or even tetramer, would not be helpful in this context.

There is the possibility that MD limitations are not the only reason for the invalidity of the H-bond hypothesis or, more in general, of MD simulations. We here show that AQP4 IgG recognizes recombinant AQP4 expressed in insect cells. However, by BN-PAGE analysis we also show that the pattern of protein aggregation in insect cells is different from that observed for AQP4 expressed in mammalian cells. In addition, AQP4 aggregates are significantly reduced after protein purification. Moreover, and most importantly, AQP4 purified from insect cells is not recognized by AQP4-IgG in ELISA sandwich. These results focus attention on a possible problem related with the non-mammalian source of AQP4 protein (either from insect cells or yeast [24,27]) used to obtain AQP4 crystal coordinates or, most likely, with the experimental procedure used to obtain the purified AQP4 crystal [24]. The hypothesis of non-mammalian source was therefore investigated in more detail using the human embryonic kidney cell line (HEK-293F), a sub-clone of the widely used HEK293 cell line, which is the most popular cell line used in the NMO field, able to grow in suspension and for this reason useful for large protein expression methods. In terms of methodology, compared to the method reported by Ho and collaborators [24], we have here used a lower imidazole concentration and we have not performed protease digestions at the end of the procedure. Despite these ameliorative changes, supposed to be more conservative of the OAP structure, we show that nickel purified AQP4 from HEK-293F cells, is not recognized by AQP4-IgG. Consequently, we can conclude that the histidine-nickel based affinity purification may be responsible for OAP supramolecular structure impairing. These conclusions suggest that AQP4 crystal may not represent the complexity of OAPs, and that MD analysis could be affected by technical artifacts. This hypothesis is supported by published MD conclusion subsequently not confirmed, such as the crystal lattice packing and relative hypothesis of AQP4-mediated cell-cell adhesion, obtained with rat AQP4, not confirmed by wet experiments conducted by cell-cell adhesion test on AQP4 expressing cells [28].

In the present study, we have provided evidence useful to understand the conformational dynamics of AQP4 epitope assembly. In particular, using the classic mutagenesis approach, we do not confirm the MD prediction that the breakdown of a H-bond between L53 and T56 is the reason for AQP4 epitope disassembly in AQP4D69H. We believe this is key information considering that the knowledge of epitope molecular characteristics is the starting point for the design of new AQP4–specific pharmacological approaches aimed at solving the pathogenic interaction between OAPs and AQP4-IgG. More in general, this study highlights the need for computational analysis to be always supported by experimental validation especially when the architecture of supra-molecular based structures is under analysis. In conclusion, given the complex nature of the AQP4 epitope, MD simulation might not be suitable for molecular medicine advances in NMO.

Conflict of interest

The authors have no conflicts of interest with the contents of this article.

Author contributions

G.P.N. conceived the study; F.P. and G.P.N designed experiments and wrote the manuscript with inputs from A.F and M.S; F.P, L.S., C.D.G., M.G.M, A.C. and G.C. conducted the experiments and performed data analysis.

Transparency document

The Transparency document associated with this article can be found, in the online version.

Acknowledgements

This work was supported by grants from the Italian Ministry of the University and Research (FIRB-Futuro in Ricerca RBFR12SJA8 to GPN; Rome, Italy), and fellowship from Apulia Region (FIR 5CU9HC5 to FP), Fondo di Sviluppo e Coesione 2007-2013 – APQ Ricerca Regione Puglia "Programma regionale a sostegno della specializzazione intelligente e della sostenibilità sociale ed ambientale – Future In Research".

The authors would like to thank Richard Lusardi for his assistance in revising the English of the article.

References

[1] G.P. Nicchia, F. Pisani, L. Simone, A. Cibelli, M.G. Mola, M. Dal Monte, A. Frigeri, P. Bagnoli, M. Svelto, Glio-vascular modifications caused by Aquaporin-4 deletion in the mouse retina, Exp. Eye Res. 146 (2016) 259–268.
[2] G.P. Nicchia, A. Rossi, M.G. Mola, F. Pisani, C. Stigliano, D. Basco, M. Mastrototaro, M. Svelto, A. Frigeri, Higher order structure of aquaporin-4, Neuroscience 168 (2010) 903–914.
[3] M.C. Papadopoulos, A.S. Verkman, Aquaporin water channels in the nervous system, Nat. Rev. Neurosci. 14 (2013) 265–277.
[4] G.P. Nicchia, F. Pisani, A. Sparaneo, M.G. Mola, D. Basco, A. Rossi, M. Svelto, A. Frigeri, Aquaporin-4 orthogonal arrays of particles from a physiological and pathophysiological point of view, Wiley Interdiscip. Rev. 2 (2013) 143–154.
[5] Y. Fujiyoshi, K. Mitsuoka, B.L. de Groot, A. Philippsen, H. Grubmuller, P. Agre, A. Engel, Structure and function of water channels, Curr. Opin. Struct. Biol. 12 (2002) 509–515.
[6] T. Walz, Y. Fujiyoshi, A. Engel, The AQP structure and functional implications, Handb. Exp. Pharmacol. (2009) 31–56.
[7] W.N. Green, Ion channel assembly: creating structures that function, J. Gen. Physiol. 113 (1999) 163–170.
[8] J.E. Rash, T. Yasumura, C.S. Hudson, P. Agre, S. Nielsen, Direct immunogold labeling of aquaporin-4 in square arrays of astrocyte and ependymocyte plasma membranes in rat brain and spinal cord, Proc. Natl. Acad. Sci. U. S. A. 95 (1998) 11981–11986.
[9] J.E. Rash, L.A. Staehelin, Freeze-cleave demonstration of gap junctions between skeletal myogenic cells in vivo, Dev. Biol. 36 (1974) 455–461.
[10] H. Wolburg, Orthogonal arrays of intramembranous particles: a review with special reference to astrocytes, J. Hirnforsch. 36 (1995) 239–258.
[11] G.P. Nicchia, M. Mastrototaro, A. Rossi, F. Pisani, C. Tortorella, M. Ruggieri, A. Lia, M. Trojano, A. Frigeri, M. Svelto, Aquaporin-4 orthogonal arrays of particles are the target for neuromyelitis optica autoantibodies, Glia 57 (2009) 1363–1373.
[12] P.W. Phuan, J. Ratelade, A. Rossi, L. Tradtrantip, A.S. Verkman, Complement-dependent cytotoxicity in neuromyelitis optica requires aquaporin-4 protein assembly in orthogonal arrays, J. Biol. Chem. 287 (2012) 13829–13839.
[13] J.M. Crane, C. Lam, A. Rossi, T. Gupta, J.L. Bennett, A.S. Verkman, Binding affinity and specificity of neuromyelitis optica autoantibodies to aquaporin-4 M1/M23 isoforms and orthogonal arrays, J. Biol. Chem. 286 (2011) 16516–16524.
[14] F. Pisani, M. Mastrototaro, A. Rossi, G.P. Nicchia, C. Tortorella, M. Ruggieri, M. Trojano, A. Frigeri, M. Svelto, Identification of two major conformational aquaporin-4 epitopes for neuromyelitis optica autoantibody binding, J. Biol. Chem. 286 (2011) 9216–9224.
[15] V.A. Lennon, T.J. Kryzer, S.J. Pittock, A.S. Verkman, S.R. Hinson, IgG marker of optic-spinal multiple sclerosis binds to the aquaporin-4 water channel, J. Exp. Med. 202 (2005) 473–477.
[16] F. Pisani, A. Sparaneo, C. Tortorella, M. Ruggieri, M. Trojano, M.G. Mola, G.P. Nicchia, A. Frigeri, M. Svelto, Aquaporin-4 autoantibodies in Neuromyelitis Optica: AQP4 isoform-dependent sensitivity and specificity, PLoS One 8 (2013), e79185. .
[17] J. Ratelade, A.S. Verkman, Neuromyelitis optica: aquaporin-4 based pathogenesis mechanisms and new therapies, Int. J. Biochem. Cell Biol. 44 (2012) 1519–1530.
[18] F. Pisani, M.G. Mola, L. Simone, S. Rosito, D. Alberga, G.F. Mangiatordi, G. Lattanzi, O. Nicolotti, A. Frigeri, M. Svelto, G.P. Nicchia, Identification of a point mutation impairing the binding between aquaporin-4 and neuromyelitis optica autoantibodies, J. Biol. Chem. 289 (2014) 30578–30589.
[19] G.P. Owens, A. Ritchie, A. Rossi, K. Schaller, S. Wemlinger, H. Schumann, A. Shearer, A.S. Verkman, J.L. Bennett, Mutagenesis of the aquaporin 4 extracellular domains defines restricted binding patterns of pathogenic neuromyelitis optica IgG, J. Biol. Chem. 290 (2015) 12123–12134.
[20] G.F. Mangiatordi, D. Alberga, L. Siragusa, L. Goracci, G. Lattanzi, O. Nicolotti, Challenging AQP4 druggability for NMO-IgG antibody binding using molecular dynamics and molecular interaction fields, Biochim. Biophys. Acta 1848 (2015) 1462–1471.
[21] M. Zuidscherwoude, F. Gottfert, V.M. Dunlock, C.G. Figdor, G. van den Bogaart, A.B. van Spriel, The tetraspanin web revisited by super-resolution microscopy, Sci. Report. 5 (2015) 12201.
[22] F. Pisani, P. Settanni, S. Rosito, M.G. Mola, R. Iorio, C. Tortorella, M. Ruggieri, M. Trojano, M. Svelto, A. Frigeri, G.P. Nicchia, Development of an aquaporin-4 orthogonal array of particle-based ELISA for neuromyelitis optica autoantibodies detection, PLoS One 10 (2015), e0143679. .
[23] K. Miyazaki, Y. Abe, H. Iwanari, Y. Suzuki, T. Kikuchi, T. Ito, J. Kato, O. Kusano-Arai, T. Takahashi, S. Nishiyama, H. Ikeshima-Kataoka, S. Tsuji, T. Arimitsu, Y. Kato, T. Sakihama, Y. Toyama, K. Fujihara, T. Hamakubo, M. Yasui, Establishment of monoclonal antibodies against the extracellular domain that block binding of NMO-IgG to AQP4, J. Neuroimmunol. 260 (2013) 107–116.
[24] J.D. Ho, R. Yeh, A. Sandstrom, I. Chorny, W.E. Harries, R.A. Robbins, L.J. Miercke, R.M. Stroud, Crystal structure of human aquaporin 4 at 1.8 A and its mechanism of conductance, Proc. Natl. Acad. Sci. U. S. A. 106 (2009) 7437–7442.
[25] L.E. LaConte, V. Voelz, W. Nelson, M. Enz, D.D. Thomas, Molecular dynamics simulation of site-directed spin labeling: experimental validation in muscle fibers, Biophys. J. 83 (2002) 1854–1866.
[26] S. Mader, A. Lutterotti, F. Di Pauli, B. Kuenz, K. Schanda, F. Aboul-Enein, M. Khalil, M.K. Storch, S. Jarius, W. Kristoferitsch, T. Berger, M. Reindl, Patterns of antibody binding to aquaporin-4 isoforms in neuromyelitis optica, PLoS One 5 (2010), e10455.
[27] Y. Hiroaki, K. Tani, A. Kamegawa, N. Gyobu, K. Nishikawa, H. Suzuki, T. Walz, S. Sasaki, K. Mitsuoka, K. Kimura, A. Mizoguchi, Y. Fujiyoshi, Implications of the aquaporin-4 structure on array formation and cell adhesion, J. Mol. Biol. 355 (2006) 628–639.
[28] H. Zhang, A.S. Verkman, Evidence against involvement of aquaporin-4 in cell-cell adhesion, J. Mol. Biol. 382 (2008) 1136–1143.